Hindawi Publishing Corporation
EURASIP Journal on Advances in Signal Processing
Volume 2011, Article ID 341836, 14 pages
doi:10.1155/2011/341836

Research Article

Particle Swarm Optimization Based Noncoherent Detector for Ultra-Wideband Radio in Intensive Multipath Environments

Bin Li, Zheng Zhou, Weixia Zou, and Wanxin Gao

Key Lab of Universal Wireless Communications, MOE, School of Information and Communication Engineering, Beijing University of Posts and Telecommunications (BUPT), P.O. Box 96, Xi Tu Cheng Road, Beijing 100876, China

Correspondence should be addressed to Bin Li, stonebupt@gmail.com

Received 11 June 2010; Revised 13 November 2010; Accepted 17 January 2011

Academic Editor: Yannis Kopsinis

Given the dense multipath propagation in typical ultra-wideband channels, traditional coherent receivers may become computationally complex and impractical. Recently, noncoherent UWB architectures have been motivated with simple implementations. Nevertheless, the rudimentary statistical assumption and practical information uncertainty inevitably results in a hardly optimistic receiving performance. Inspired by the nature processes, in this paper we suggest a noncoherent UWB demodulator based on the particle swarm intelligence which can be realized in two steps. Firstly, a characteristic spectrum is developed from the received samples. From a novel pattern recognition perspective, four distinguishing features are extracted from this characteristic waveform to thoroughly reveal the discriminant properties of UWB multipath signals and channel noise. Subsequently, this established multidimensional feature space is compressed to a two-dimension plane by the optimal features combination technique, and UWB signal detection is consequently formulated to assign these pattern points into two classes at the minimum errors criterion. The optimal combination coefficients and the decision bound are then numerically derived by using the particle swarm optimization. Our biological noncoherent UWB receiver is independent of any explicit channel parameters, and hence is essentially robust to noise uncertainty. Numerical simulations further validate the advantages of our algorithm over the other noncoherent techniques.

1. Introduction

The fast growing interest in ultra-wideband (UWB) has been stimulated by the attractive features including low probability of detection (LPD), low power consumption and low-scomplexity baseband operations [1, 2]. Due to its potential that provides an extremely high data rates even surpassing 1 Gbps, UWB has long been considered as a promising candidate for high-speed transmissions in wireless personal area networks (WPANs) [3, 4], mainly for the online broadband multimedia stream services in short range applications (10–15 m). Meanwhile, with its outstanding capability of positioning and material penetrating (e.g., the foliage and walls), UWB has intensive military applications, such as the high-resolution ground penetrating radars (GPRs), through-wall imaging, and precise navigation [5, 6]. Most recently, the emerging body area networks (BANs) also consider UWB radios as an appealing resolution for health monitoring [7], due to its simple implementations and extremely low radiation.

Impulse radio (IR) is one of physical proposal for UWB communications, in which the information bit is directly coded into a set of short-duration baseband pulses [1, 8]. If the principle of UWB-IR is taken into account, without the complicated radio frequency (RF) front-end, the low-complexity transmitter seems to be feasible generally. Nevertheless, owing to the enormous bandwidth of emission pulses which even may be up to several gigahertz (GHz), signal processing for UWB receivers has been remained as formidable challenges in the presence of the highly dispersive propagations [9–11]. So, those traditionally derived optimal coherent receivers may be not applicable for UWB systems in three considerations [12]. First, synchronization in coherent receivers must be accomplished at the scale of subnanosecond duration, which requires sophisticated algorithm and low clock jitter hardware [9]. Second, in order

to accurately extract the amplitude and position of each resolvable multipath component, the highly computational complexity of channel estimation is usually unaffordable [13, 14]. Third, the coherent RAKE architecture integrating a great population of fingers (correlator) leads to the impractical hardware structure [15, 16].

To deal with these challenges, the transmitted-reference (TR) structure is introduced in [17] to simplify UWB receives, in which a pair of pulses are simultaneously emitted, with the first pulse serving as the multipath channel template for the second information-bearing one. It is obvious that the transmission efficiency in TR is reduced by 50% due to the reference signaling. Although special TR schemes have been developed to compensate the transmission efficiency [18, 19], the analog delay lines in TR are still difficult to realize with the requisite accuracy. Recently, energy detection (ED) based noncoherent receivers have been motivated with the simple implementations [12, 20, 21]. Not depending on the channel impulse response (CIS), channel estimation as well as RAKE structure can be avoided [12]. Moreover, the noncoherent architectures are virtually immune to the clock timing estimation errors, compared to the precise timing requirement in coherent receivers typically of ± 10 ps [22], which further make the low complexity UWB devices possible. Given that no channel characteristic has been exploited, nevertheless, the performance of this suboptimal alternative is still far from being satisfactory. Besides, ED is significantly vulnerable to the noise uncertainty caused by the fluctuated in-band noises [23]. Considering it is practically impossible to know the accurate noise power, so inevitably its performance may degrade noticeably.

In the last two decades, many advances on computer science and engineers have been based on the observations and the emulations of the natural world processes. Biological inspired algorithms are problem-solving techniques that attempt to simulate the occurrence of natural processes, such as the evolution of species [24], organization of insect colonies [25] and the working of immune systems [26]. Particle swarm optimization (PSO) is one evolutionary computation technique combining the *social psychology* principles in *sociocognition* human agents and evolutionary computation [27, 28], which is motivated by the social behavior of organisms such as fish schooling and bird flocking. PSO comprises a simple concept and can be conveniently implemented by using some primitive mathematical operators, which is computationally efficient in terms of memory and speed [27]. PSO benefits from the past experience of the particle population. Interaction within the group gives a tug toward the good solution [27]. It has been reported that PSO has advantages over genetic algorithm (GA) for efficiently finding the optimal or near-optimal solutions [29]. One of the most extensively investigated application of PSO in communication engineering is the multiuser detection (MUD) in code division multiple access (CDMA) systems. The PSO-MUD algorithm initialized by the conventional LMMSE detector was proposed in [30]. Recent researches also applied PSO techniques to the minimum bit error rate (MBER) multiuser transmitter designing and the MUD receiver-diversity in space-time block-coding (STBC) systems [31, 32]. In [33], Zhao employed PSO to optimize the resources allocation in orthogonal frequency division multiplexing (OFDM) system in the context of cognitive radios (CRs). Currently, it seems that PSO-based signal processing schemes mainly focus on certain limited areas mentioned above, for example, the MUD and the multiobjectives optimization in resources allocation, in which PSO essentially serves as an optimal tool for these classical formulated modeling. From this perspective, therefore, extensive PSO applications in signal detection may still remain to go deep into.

Our main contribution is that, in this paper, we design a novel noncoherent UWB detector based on PSO from an attractive pattern classification aspect, which provides an insight to more general biological inspired signal processing. Firstly, we establish a novel *characteristic spectrum* from the received samples blindly through a sequence of signal conversions. Enlightened by the discriminant shaping of the derived characteristic spectrums, four distinguished features are then extracted to comprehensively reflect the intrinsic differences between the UWB multipath signals and the additive channel noise. After the partial feature combinations, for the first time, UWB signal detection is transformed to a two-class *pattern recognition* problem in a two-dimensional feature plane. Furthermore, we show from simulation derivations that excess detection gain can be achieved if PSO is adopted to fuse these correlated features in a constructive fashion by optimal feature combination scheme (OFC). The optimal division bound in the formed 2D plane is also obtained finally by resorting to PSO. Our nonparametric algorithm significantly enhances the detection performances, compared with the noncoherent ED receiver which is served as the benchmark in consideration of exploiting no prior channel information. Not relying on explicit channel parameters, this suggested scheme is also practically immune to noise uncertainty. Generally, our suggested bioinspired algorithm for UWB receivers may extend PSO to a much wide application prospect, which largely benefits the future related researches.

The remainder of this paper is outlined as follows. In Section 2, we depict the indoor UWB channel characteristic and formulate the noncoherent detection problem in UWB systems. We then develop a novel algorithm in Section 3 to analyze the received multipath signals. Based on the derived characteristic spectrum, we employ two patterns in a 2-D plane to represent two channel states. Section 4 is then dedicated to numerical simulations. The performance evaluation of our suggested UWB receivers is also presented in this part. Finally, we conclude the whole paper in Section 5.

2. Indoor UWB Channel

UWB radio technique generally characterizes signals whose fractional bandwidth (i.e., its 3 dB bandwidth divided its center frequency) is large, typically over 0.25, or its instantaneous spectral occupancy exceeds 500 MHz [2, 34]. Avoiding the adoption of local oscillators or frequency mixers, UWB emission signals can be usually generated by driving an

antenna with the extremely short pulses whose duration is on the order of a few nanoseconds (ns) to fractions of a nanosecond. So, such a UWB technique is often referred to as short pulse or impulse radio systems [1].

2.1. Short-Range UWB Channel. Owing to the large bandwidth of emission waveforms, the ability of UWB receivers to resolve the different reflections in the channel has been greatly enhanced, which is in striking contrast to traditional narrowband systems. Accordingly, the realistic UWB channels exhibit two following distinctive characteristics [9–11]. First, the number of reflections arriving within the period of a very short impulse (e.g., nanosecond) becomes much smaller as the duration of the impulse gets shorter. According to the centre limit theory [35], therefore, the distribution of the received signal envelope caused by the channel trajectories may *not* be described by the Rayleigh fading model as in most narrowband channels [36]. Second, since the multipath components may be resolved at a very fine time scale, the time of arrival (TOA) of multipath components may not be continuous. As multipath trajectories may result from reflections off walls, ceilings, furniture, and other large objects, consequently, different objects could contribute to different "*clusters*" of multipath components, which has also been confirmed by measurements. This phenomenon is firstly reported by the well known Saleh-Valenzuela (S-V) channel model [11].

In this paper, we adopt UWB channel modeling regulated in [37] by IEEE 802.15.3a Task Group, which is based on the modified S-V model [11]. Four standard channel models are defined for UWB indoor applications in different dense multipath propagations; those are CM1, CM2, CM3, and CM4. The expression of the channel impulse response can be given by:

$$h(t) = X\sum_{l=0}^{L-1}\sum_{m=0}^{M-1}\alpha_{m,l}\delta(t - T_l - \tau_{m,l}), \tag{1}$$

where L denotes the number of clusters, M is the number of rays of each cluster, $\alpha_{m,l}$ is the fading coefficient of the mth path of the lth cluster, X is the channel fading factor, T_l is the arrival time of the lth cluster, and $\tau_{m,l}$ is the delay of the mth path of the lth cluster relative to T_l. T_l and $\tau_{m,l}$ have a Poisson distribution, and $\alpha_{m,l}$ and X are log-normal random variables [10, 37]:

$$\begin{aligned} p(T_l \mid T_{l-1}) &= \Lambda\exp[-\Lambda(T_l - T_{l-1})], \quad l > 0, \\ p(\tau_{k,l} \mid \tau_{k-1,l}) &= \lambda\exp[-\lambda(\tau_{k,l} - \tau_{k-1,l})], \quad k > 0. \end{aligned} \tag{2}$$

We also assume UWB multipath channel to be quasistatic in our analysis, which means the amplitude coefficients $\alpha_{m,l}$ and delays $T_l + \tau_{m,l}$ remain invariant over one transmission burst, but are allowed to change across bursts. For the purpose of elaborations simplicity, we may equal the multipath channel to be a tapped-delay line with L_{td} taps and delays

$$h(t) := \sum_{l=0}^{L_{td}}\alpha_l\delta(t_l - \tau_l). \tag{3}$$

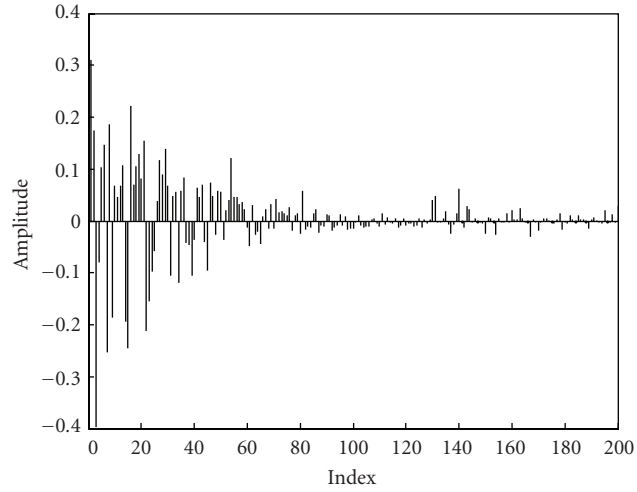

Figure 1: UWB channel impulse response of the light of sight (LOS), 1–4 m.s.

Figure 1 illustrates one typical realization of the UWB indoor channel generated by using the 802.15.3a modeling in the CM1 case.

2.2. UWB Transmitter. Considering that we mainly deal with noncoherent detection in this work, UWB transmitter should also take the limitations of the receiver infrastructure into consideration, in which the phase information may be totally lost since no attempt of recovering multipath channel responses is made [12]. As a result, phase modulation schemes become invalid for a noncoherent receiver.

We employ the time-hopping pulse position modulation (TH-PPM) in our analysis. The corresponding signal format is described by [1, 8]

$$x(t) = \sqrt{\frac{E_b}{N_s}}\sum_{i=0}^{P-1} w\left(t - iT_f - c_iT_b - d_{\lfloor i/N_s\rfloor}\delta\right), \tag{4}$$

where $\lfloor x\rfloor$ gives the biggest integer smaller than x. E_b is the bit energy, N_s is the number of pulses used to represent one bit, T_b is the bit period of a single bit, $d(i)$ $(i = 0, 1, 2\ldots, P-1)$ are the transmitted data of length P taking values of $\{0, 1\}$, T_f is the time period of a frame, c_i is the time-hopping code and δ is the bit separation time interval for one PPM symbol. $w(t)$ represents the generally adopted spectrum shaper for UWB communications, for example, the Gaussian pulse and the high-order derivation of Gaussian pulse [2].

2.3. Coherent Receiver. Within the current RAKE framework, based on the accurately estimated multipath channel response, the resolvable trajectories could be coherently combined to provide the appealing multipath diversity, further making UWB immune to channel fading [38]. However, as is indicated by most investigations, the number of resolvable multipath may even approach 70–80 in order to accumulate 85% dispersed channel energy, which can be also clearly seen from Figure 1. As a result, the widely adopted coherent architectures face a couple of technical challenges.

The efforts to compute both the position and amplitude of so many multipath components become computationally unaffordable in terms of the algorithm complexity and speed [39]. Moreover, the required number of correlator is huge, and hence, the integration implementation tends to be impractical [40].

As one suboptimal alternative, on the other hand, TR structure has recently excited great interest. In TR, the first pulse carries no information and is only used as the multipath template/reference for demodulation of the second pulse. It is clearly seen that considerable transmission power should be relocated to the first reference pulse. More importantly, the analog delay lines in TR may prevent them from precise realization, resulting in remarkable performance degradation. Considering no effort to recover the multipath components is made, the author in [12] groups TR into noncoherent receivers. In this paper, nevertheless, we still view it as a *partial coherent* technique based on two considerations. First, the reference pulse in traditional TR aims at providing channel template to the second information-bearing pulse. So, channel estimation is accomplished in a relatively vague manner. Second, PSK modulation is always adopted in the second pulse, which keeps in collision with the principle of noncoherent techniques [41].

2.4. Noncoherent Receiver. Based on the implementation motivations, it is easy to recognize that those well-established receiving algorithms derived for narrowband systems are not feasible for UWB anymore. Perusing for the low complexity and low power UWB architectures, alternatively, current studies have been slowly shifted to the suboptimal and noncoherent structures such as ED [12, 21].

The decision variable in ED is only related with the received signal power and the channel noise power; therefore, channel estimations and RAKE fingers are not necessary, which is of significance to the concise UWB structures. Supposing the received signal is denoted by $y(n)$, $n = 0, 1, \ldots, N-1$, then for OOK scheme, we have,

$$Y_{\mathrm{ED}} \triangleq \sum_{n=0}^{N-1} y^2(n) = \begin{cases} \sum_{n=0}^{N-1} (h(n) + w(n))^2 & H_1, \\ \sum_{n=0}^{N-1} w^2(n) & H_0. \end{cases} \tag{5}$$

Here, $w(m)$ is the additive white Gaussian noise (AWGN) with zero mean and variance σ_w^2. The test statistics Y_{ED} follows a central chis-quare distribution with $2N$ degrees of freedom under H_0, and a noncentral chisquare distribution with $2N$ degrees under H_1 [21, 35].

So, when it comes to noncoherent detectors, signal demodulation is to identify whether there is sufficient signal power available in current time window. Even for TH-PPM scheme in (4), we may still divide the symbol duration into multiple time bins according to the *bit separation interval*, and correspondingly, PPM signal detection is to in parallel determine which subbin contains sufficient signal energy.

Since little prior channel information can be exploited in ED except for signal power, its detection performance is generally uncompetitive. Moreover, due to the noise uncertainty caused by the variations of both thermal and environment noises, practically it is very difficult to obtain the accurate noise power σ_w^2. Induced by this *information imperfection*, as a result, ED usually experiences serious performance decline. Recently, a novel UWB structure is proposed in [42, 43], in which the received samples $y(n)$ are firstly weighted by the average power decay profile (APDP) of UWB multipath channels and then form the decision variable Y_{APDP}. By constructively exploring this partial channel information state (CSI), the APDP performance can be improved by 1–3 dB compared with ED [42]. However, for the geographically widespread and distributed UWB sensor networks, as is in most realistic applications, this partial CSI is hardly to get without a great mass of information exchange between the network cluster head (CH) and local UWB nodes [41]. From this aspect, APDP belongs to a *semicoherent* method essentially. Therefore in our following analysis, we mainly adopt ED as the benchmark of noncoherent UWB receiver for performance evaluations.

Notice that we denote the received UWB multipath signal by the discrete channel response $h(n)$ for elaborations simplicity, in which we assumes the precise synchronization has been achieved and the sampling frequency is equivalent to the *Nyquist* rate. Nevertheless, it is noteworthy that sampling requirements on ADC is relatively loose in noncoherent receivers, so down-Nyquist rate is also practicable [12].

3. Noncoherent UWB Receiver Design

Generally, according to the classical Bayesian decision theory, the statistics assumptions and formulations may lead to the optimal solution in most engineering applications, if the complete and accurate probability information is available [36]. For some specific applications especially the noncoherent UWB demodulators considered above, however, the assumed information (e.g., the probability density function of the summed energy Y_{ED}) is rather rudimentary. Additionally, the performance is relatively immune to the practical information imperfection, for example, the noise uncertainty.

On the other hand, careful observations on nature processes indicate that the biological activities can solve the problems encountered in daily life in a much effective way. For example, human can exactly differentiate/recognize one thing from others through certain elegant characteristics which are evolutionarily learned by self-training. Usually, the achieved decisions are far superior to what we can achieve with our current engineering knowledge and methods, especially for the nonideal situations in the presence of information limitations and uncertainties. Inspired by the nature mechanics, we deal with UWB noncoherent receiving as a *state recognition problem* in this work. We firstly develop a novel characteristic spectrum from the received signals to comprehensively represent the intrinsic properties of the two channel states H_1 and H_0. Then, a set of distinguished quantifiable features is constructed from this characteristic waveform. By utilizing PSO algorithm, the high-dimensional features space is advantageously mapped to a 2-D plane

in which the optimal division bound is determined from numerical optimization. Based on this presented biological algorithm, we can accurately isolate UWB multipath signals from the channel noise even if no prior probability is assumed and the information imperfection is taken into account.

Starting from the noisy received waveform $y(n)$, our scheme includes four steps in order to establish the features space. (1) Construct the autocorrelation matrix and derive characteristic spectrum, (2) extract the multiple features, (3) combine the correlated features and form a 2-D decision plane; and (4) derive the optimal combination coefficients and the decision bound using PSO.

3.1. Construct the Characteristic Spectrum. Given the observed signals consisting of N samples which is denoted by a vector $y(n)$ $(n = 0, 1, 2, \ldots, N-1)$, we may firstly construct an autorelation matrix $\mathbf{A}$ according to

$$\mathbf{A} = \mathbf{y}^T\mathbf{y}. \tag{6}$$

In order to fully exploit the more profound statistic information of multipath channels, we perform the matrix transformation on $\mathbf{A}$

$$\mathbf{B} = \mathbf{A}^T\mathbf{A}. \tag{7}$$

We denote the principal diagonal elements of $\mathbf{B}$ by $\boldsymbol{\beta}$, while the elements immediately below this diagonal by $\boldsymbol{\rho}$. Alternatively, $\boldsymbol{\rho}$ can be regarded as the diagonal elements of a dimension-decreased matrix which corresponds to the cofactor of $B(N, N)$ [44]

$$\boldsymbol{\beta}_{1\times N} = \mathrm{diag}(\mathbf{B}) = B(i,i), \quad i = 0, 1, 2, \ldots, N-1, \tag{8}$$

$$\boldsymbol{\rho}_{1\times(N-1)} = \mathrm{diag}(\mathbb{B}) = B(i+1,i), \quad i = 0, 1, 2, \ldots, N-2. \tag{9}$$

The characteristic spectrum of the received signals can be now defined as the *correlation function* between $\boldsymbol{\beta}$ and $\boldsymbol{\rho}^2$. Here, the nonlinear process on $\boldsymbol{\rho}$ is necessary to obtain multiple features from this characteristic waveform

$$\mathbf{c}_{1\times(2N-2)} = \boldsymbol{\beta} \odot \boldsymbol{\rho}^2, \tag{10}$$

where $\odot$ represents the linear correlating process [36]. We denote the received multipath UWB signals disrupted by the channel noise by $y_1(n)$ $(n = 0, 1, 2, \ldots, N-1)$ when the channel state is H_1. Then, according to (6)–(10), we may easily derive the expression of the characteristic spectrum under H_1

$$c(k) = \begin{cases} E_r^3 \displaystyle\sum_{i=0}^{k-1} y_1^2(i)\, y_1^2(N-1-k+i)\, y_1^2(N-k+i), \\ \qquad\qquad k = 1, 2, \ldots, N-1, \\ E_r^3 \displaystyle\sum_{i=0}^{2N-1-k} y_1^2(k-N+1+i)\, y_1^2(i)\, y_1^2(1+i), \\ \qquad\qquad k = N, N+1, \ldots, 2N-1. \end{cases} \tag{11}$$

Here, E_r is the total received energy. According to the property of UWB multipath channels, the power decay profile can be reasonably approximated by the exponential function [21, 41], which contains two parts, that is, the noise item and the determined item

$$y_1^2(k) \simeq \exp\left(-\frac{k}{\tau}\right) + N_1 w_1(k) + B_1, \quad k = 0, 1, 2, \ldots, N-1, \tag{12}$$

where τ is related with the specific channel configurations, that is, the root mean square (RMS) delay. B_1 and N_1 denote the noise mean and variance of $y_1^2(k)$, respectively, which are both connected with the channel noise power σ_w^2. $w_1(k)$ denotes a white exponential random process. Accordingly, we may further approach $y_1^4(k)$ by

$$y_1^4(k) \simeq \exp\left(-\frac{2k}{\tau}\right) + N_2 w_2(k) + B_2, \quad k = 0, 1, 2, \ldots, N-1. \tag{13}$$

Notice that for a good channel condition with low noise power, we may further have:

$$y_1^2(i)\, y_1^2(1+i) \simeq C_0\, y_1^4(i), \quad i = 1, 2, \ldots, N, \tag{14}$$

where C_0 is a constant also related with channel configuration, which approaches 1 in practice.

We note that the noise components in (13) and (14) are both originated from $w(k)$ in (5), so they are obviously correlated with each other. (1) The correlation coefficient ρ_w between $w_1(k)$ and $w_2(k)$ is relatively high, which may approach 1 in practice. (2) On the other hand, as the variables derived from independent random variables $w(k)$ also keep independent of each other, the correlation between $w_1(k)$ and the shifted $w_2(k)$, denoted by $\tilde{w}_2(k)$, basically approaches zero. Based on these two points above, with little manipulation efforts and by removing the constant item, we further obtain the expression of $c(k)$

$$c(k) = \sum_{i=0}^{k-1} \exp\left(-\frac{i + 2\times(N-k+i)}{\tau}\right) + \nu_k + C_k, \quad k = 1, 2, \ldots, N, \tag{15}$$

where % represents the modulus operator. ν_k represents the Gaussian random variable. The variable C_k in (15) is given in (16). Notice that for the remaining values of k (e.g., $k = N+1, \ldots, 2N-1$), the expression of $c(k)$ is much similar to (15), only with the summation range replaced by $[k-N+1,\ N]$, and the variable k in (16) by $2N-1-k$

$$C_k \approx \begin{cases} B \displaystyle\sum_{i=0}^{k-1} \exp\left(-\frac{2\kappa_i}{\tau}\right) + B_1 \sum_{i=0}^{k-1} \exp\left(-\frac{i}{\tau}\right) \\ \qquad + kB_1B_2, \quad k \neq 1, \\ B \displaystyle\sum_{i=0}^{k-1} \exp\left(-\frac{2\kappa_i}{\tau}\right) + B_1 \sum_{i=0}^{k-1} \exp\left(-\frac{i}{\tau}\right) \\ \qquad + kB_1B_2 + \rho_w k N_1 N_2, \quad k = 1. \end{cases} \tag{16}$$

Here, ρ_w denotes the correlations coefficient between $w_1(k)$ and $w_2(k)$, and κ_i is equivalent to $N-k+i$. From (15) and (16), it is clearly found that $c(k)$ is also a Gaussian random process with its mean and variance related with k. For the complete channel noise H_0, we can also obtain the corresponding characteristic spectrum in a similar manner. Based on numerical computations, the waveforms of $c(k)$ are illustrated in Figures 2(a) and 2(b), respectively corresponding to the UWB multipath signals (H_1) and the complete channel noise (H_0).

We note that $c(k)$ are clearly distinctive under the two channel states H_1 and H_0. In order to highlight this characteristics waveform, we employ a moving average (MA) filter to further smooth $c(k)$. Empirically, an appropriate length for this average process is about $N/5$. The final obtained characteristic waveform, denoted by $d(k)$, is also depicted in Figures 2(a) and 2(b). After this smoothing process, the distinguishing characteristics have become much more conspicuous, based on which certain quantifiable features can be conveniently developed to effectively separate UWB signals from the channel noise. From this point of view, we may have every reason to refer to $d(k)$ (or $c(k)$) as the *characteristic spectrum*.

3.2. Establish the Feature Space. It is apparently found many discriminant aspects in the character waveforms from Figures 2(a) and 2(b). In order to establish the quantifiable characteristics space that can identify two channel hypotheses in (5), we may choose the following prominent features.

(1) If we define the area below $d(k)$ as the *equivalent energy*, then we may note this energy item is quite concentrated at the centre range of the characteristic waveform when the UWB multipath signals have been assumed (i.e., H_1). While this equivalent energy is relatively dispersed with only channel noise (i.e., H_0). As a result, we define the first feature as

$$F_1 = \frac{\sum_{k=N-1-K}^{N-1+K} d(k)}{\sum_{k=0}^{2N-1} d(k)}. \tag{17}$$

The range of interest in (17) is limited by the key parameter K. Practically, K can be determined by the imbalance property of $d(k)$. That is, K can be immediately obtained once the right value $d(N-1+K)$ has surpassed the left value $d(N-1-K)$ by δ. A simple and practical strategy is directly set δ to 0

$$K = \min_k \arg\{d(N-1+k) - d(N-1-k) > \delta\}. \tag{18}$$

(2) It is noticeable that, in Figure 2(a), the change rate of characteristic waveform in the middle range is much faster than that of in Figure 2(b). Consequently, the variance in this range is also supposed to be much distinctive

$$F_2 = \sum_{k=N-1-K}^{N-1+K} \left(d(k) - \frac{1}{2K+1} \sum_{k=N-1-K}^{N-1+K} d(k) \right)^2. \tag{19}$$

(3) From Figure 2, the equivalent energy also exhibits remarkable imbalance during the outside range. Specifically, the right range energy is much larger than the left in the presence of UWB multipath signals, while these two parts are basically equivalent under the channel state H_0. Therefore, we can reasonably adopt this imbalance property as the third feature

$$F_3 = \sum_{k=N-1+K}^{2N-1} d(k) - \sum_{k=1}^{N-1-K} d(k). \tag{20}$$

(4) Up to now, we have focused on the properties of characteristic waveform $d(k)$, in which the received signal power has been removed by the average smoothing processing. However, this energy item can be also utilized to differentiate the two channel states, as is in ED. Therefore, we still add it into our feature set.

$$F_4 = \sum_{k=0}^{N-1} y^2(k). \tag{21}$$

By taking full advantage of the developed characteristic spectrum, we have constituted a feature set which is dedicated to separating the two channel states. It is noteworthy that although we have assumed some numerous properties and also introduced certain representation parameters in our elaborations (e.g., B_1 and N_1), no explicit channel-related parameter is employed in the derivation process of our characteristic space. Therefore, our algorithm is only related with the channel state (H_1 and H_0), other than the specific quantifiable channel parameters, such as channel noise power.

3.3. Optimal Feature Combination. Based on the already established characteristic space, an intuitive strategy is to represent each received signal with a single pattern point in this multidimensional feature space. Accordingly, UWB demodulation can be formulated to determine a *hyperplane* dividing two group data points at the minimum classification errors. This optimization problem can be solved by the support vector machines (SVM) technique according to the supervised training technique [45]. With the aid of pilot synchronization sequences during each frame, we can further derive the optimal decision bound through numerical training process. However, this highly dimensional classification problem is computationally complex generally [46], which may be not applicable to the high-speed UWB transmissions.

As a feasible alternative, we may firstly reduce the corresponding problem dimension by resorting to the feature combination technique following (22). Then, this pattern classification can be efficiently settled on this compressed 2-D F_x-F_y plane. For the popular SVM strategy, in the

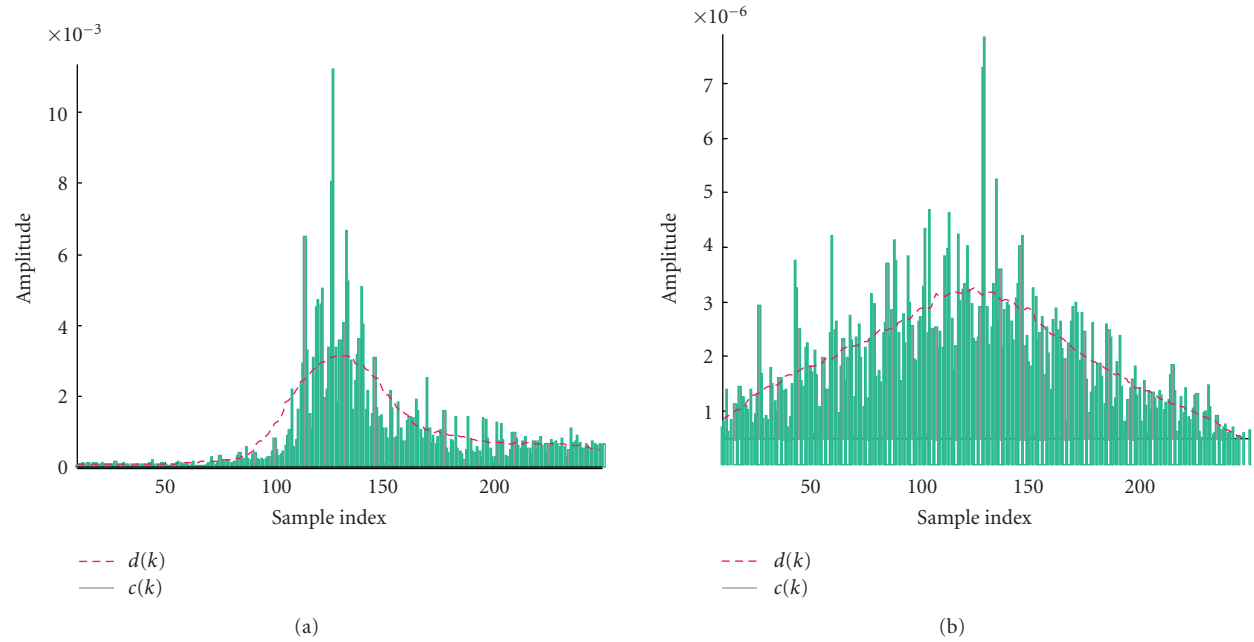

FIGURE 2: Waveforms of the derived characteristic spectrum. Notice that the E_b/N_o in simulation is set to 14 dB. (a) With the UWB multipath signals plus channel noise. (b) With only channel noise.

simplest way, we may employ the *equal ratio feature combination* (*ERFC*) technique as in (22), in which η_i is basically equivalent to $1/\text{mean}(F_i)$

$$\begin{aligned} F_x &= F_4, \\ F_y &= \eta_1 F_1 + \eta_2 F_2 + \eta_3 F_3. \end{aligned} \tag{22}$$

On the other hand, nevertheless, the derived multiple features may inevitably keep *correlated* with each other. Hence, the combination coefficients, η_i $(i = 1, 2, 3)$, could play a leadership role in the final classification or recognition performance. It is apparent that in practice, a nonoptimal feature combination may considerably undermine the discriminant property of two formed patterns in originally multidimensional space, resulting in a rather deteriorated detection performance in this dimension-reduced space. Instead, for the optimal noncoherent receiver, a group of well-designed feature combination coefficients should be used to increase the discriminant distance in F_x-F_y plane to the maximum, and hence significantly enhance the final demodulation performance. This process can be therefore referred to as the *optimal feature combination* (*OFC*), in which each combination coefficient η_i will be thoroughly optimized with the objective of minimizing the total classification errors. It is noted that these optimal combination coefficients can be practically determined by using the numerical search, as the analytic derivations may always include intractable mathematical expressions.

Other than the modification of combination coefficients η_i during OFC process, the decision bound function $f(F_x, F_y)$ also needs optimization in order to achieve the minimum recognition errors. To simplify algorithm complexity and simultaneously ensure the generalization ability, we may further specify the decision bound on 2-D feature plane to be either a *linear* function

$$f\left(F_x, F_y\right) := a_1 F_x - F_y + a_2, \tag{23}$$

or a *quadratic* function

$$f\left(F_x, F_y\right) := a_1 F_x^2 + a_2 F_x + a_3 F_x F_y + a_4 F_y. \tag{24}$$

Hence, the parameters a_i of decision bound functions can also be refined. Then, our objective of the whole optimal process is to minimize the detection errors P_e in (25), given the pilot data set with a length of M, by cautiously optimizing the combination coefficients together with the decision bound.

$$\begin{aligned} P_e = \frac{1}{M}\Bigg[&\text{num}\left(f\left(\mathbf{F}_x^0, \sum_{i=1}^{3} \eta_i \mathbf{F}_i^0\right) > 0\right) \\ &+\text{num}\left(f\left(\mathbf{F}_x^1, \sum_{i=1}^{3} \eta_i \mathbf{F}_i^1\right) < 0\right)\Bigg], \end{aligned} \tag{25}$$

where $\mathbf{F}_i^0 \in \mathbf{R}^{M\times 1}$ represents the ith feature vector constructed from the received pilot sequences under H_0, while $\mathbf{F}_i^1 \in \mathbf{R}^{M\times 1}$ is under H_1. $\text{num}(\mathbf{g})$ denotes the total number satisfying the specified condition $\mathbf{g}$. Given the mathematic formulations in (25), this numerical optimization may be generally beyond capability of those traditional algorithms, such as the SVM technique in which the critical combination coefficients η_i (e.g., OFC process) may not be further adjusted. Additionally, as the length of the training sequences (i.e., M) increases, the computational complexity of this second-order programming (SOP) based technique may also become unbearable for realistic applications [31, 45].

3.4. PSO-Based Demodulation

3.4.1. Elements of PSO. Similar to the most other evolutionary algorithms, PSO conducts its solution searching by employing a population of particle swarms, and each particle represents a potential solution. The single particle will keep track of the position of its individual best solution (*pbest*) and the global best solution (*gbest*) among the achieved *pbests* of all swarms. By combining the cognition model and social model [47], the particles are accelerated toward *pbest* and *gbest* over the iterations. The cognition model emphasizes private thinking from its own previous experience of the particle itself. While the social model represents collaborations of all the particles toward *gbest*, according to the belief of the best experience of the population.

The basic elements of PSO algorithm for the UWB noncoherent detector can be defined as follows.

(1) Population size N_P: it gives the number of the particle swarms employed in PSO.

(2) Particle $\mathbf{x}_d^i$: it represents a candidate solution denoted by a $Q \times 1$ dimensional vector. The dth particle position at the ith iteration is defined as $\mathbf{x}_d^i = [x_{d1}^i, x_{d2}^i, \ldots, x_{dQ}^i]$, where x_{dq}^i gives the position of the qth parameter of the dth particle. For the linear decision bound case, Q is 5 in this work, whereas for the quadratic bound Q is 8.

(3) Particle velocity $\mathbf{v}_d^i$: the velocity of the moving swarms represented by a $Q \times 1$ dimensional vector. The particle velocity of the dth particle at the ith iteration is defined as $\mathbf{v}_d^i = [v_{d1}^i, v_{d2}^i, \ldots, v_{dQ}^i]$, where v_{dq}^i is the velocity of the qth parameter of the dth particle.

(4) Inertia weight w_i: it can be used to reflect the influence of the velocity of previous iterations on the current velocity. Practically, it tries to balance the global and local exploration abilities of the particles [48].

(5) Maximum velocity $\mathbf{v}^{\max}$: the velocity of each swarm is limited by the maximum velocity $\mathbf{v}^{\max} = [v_1^{\max}, v_2^{\max}, \ldots, v_Q^{\max}]$, where $v_q^{\max}$ refers to the maximum velocity of the qth parameter. It is noted that $\mathbf{v}^{\max}$ can determine the resolution or fineness of PSO.

(6) Objective function F: we utilize the detection/recognition error rate in (25) as the PSO fitness

$$F(\mathbf{x}) = \arg\min_{\mathbf{x}}(P_e). \tag{26}$$

(7) Individual particle best $pbest_d^i$. The individual best solution of the dth particle at the ith iteration is denoted as $pbest_d^i$, which should fulfill $F(pbest_d^i) \leq F(\mathbf{x}_d^j)$ for all $j \leq i$.

(8) Global best $gbest^i$.$gbest^i$ is the global best particle position among all the individual best particle positions $pbest_d^i$ at the ith iteration such that $F(gbest^i) \leq F(pbest_d^i)$ for $d = 1, 2, \ldots, N_P$.

3.4.2. PSO-Based UWB Detector. Based on the ingredient knowledge of PSO algorithm, the steps of PSO-based UWB noncoherent receiver can be described as follows.

Step 1 (characteristic space construction). Conduct signal transforms on the received signal $\mathbf{y}$ according to (6)–(10). Then, extract the feature vectors based on (17)–(21).

Step 2 (swarm initialization and evaluation). With the iteration counter $i = 0$, the initial position $x_{dq}^0 (d = 1, 2, \ldots, N_P)$ is randomly generated from the range $[-30, 30]$. Set $pbest_d^0 = \mathbf{x}_d^0$ and evaluate $F(pbest_d{}^0)$. $pbest_{\min}^0$ is denoted as the individual best position such that $F(pbest_{\min}^0) \leq F(pbest_d^0)$ for $d = 1, 2, \ldots, N_P$. Set $gbest^0 = pbest_{\min}^0$. The initial velocity v_{dq}^0 is randomly chosen from $[-v_q^{\max}, v_q^{\max}]$.

Step 3 (swarm update). Firstly, we update the inertia weight w. The decrement function for decreasing the inertia weight is given as

$$w^i = \alpha w^{i-1}, \tag{27}$$

where α is the decrement constant, which is usually smaller than 1 [48]. In [49], various combinations of α and w has been studied. It is shown that the promising performance can be achieved when w and α are both close to 1. As is suggested by (27), at the initial search stage, a large inertia weight is used to enhance the global exploration, whereas for the late iterations, the inertia weight should be gradually reduced for the better local exploration.

The velocity of the qth parameter of the dth particle at the ith iteration is then changed by

$$\begin{aligned} v_{dq}^i = {} & w^i \times v_{dq}^{i-1} + c_1 \times r_1 \times \left(pbest_{dq}^{i-1} - x_{dq}^{i-1}\right) \\ & + c_2 \times r_2 \times \left(gbest_q^{i-1} - x_{dq}^{i-1}\right). \end{aligned} \tag{28}$$

In order to avoid excessive roaming of particles beyond the search space, the velocity v_{dq}^i should be bounded by the maximum velocity $v_q^{\max}$

$$v_{dq}^i = \begin{cases} v_{dq}^i & \text{If } v_{dq}^i \in [-v_{\max}, v_{\max}], \\ v_{\max} & \text{If } v_{dq}^i > v_{\max}, \\ -v_{\max} & \text{If } v_{dq}^i < -v_{\max}. \end{cases} \tag{29}$$

In (28), the first term accounts for the influence of the previous velocity to the current velocity. The second term corresponds to the cognition part, and the third term is the social part. Thus, (28) calculates the particle's current velocity according to its previous velocity, the distance of its current particle position from its own individual best particle position *pbest*, and the global best particle position *gbest*. r_1 and r_2 are both random numbers that are uniformly distributed between 0 and 1, that is, $r_i \sim U[0, 1]$ $(i = 1, 2)$.

c_1 and c_2 are the *acceleration coefficients*, respectively, corresponding to the weighting of the *stochastic* acceleration terms to pull the particle to *pbest* and *gbest* [48]. Specifically,

low values of c_1 and c_2 allow particles to roam far from target regions before being tugged back, whereas high values lead to abrupt movement toward or past the target region. A commonly adopted strategy is set both c_1 and c_2 to a constant. In our case, both c_1 and c_2 can be appropriately set to 2. Nevertheless, it was reported in [50] that using a time varying acceleration coefficient (TVAC) enhances the performance of PSO. So, we may also adopt this mechanism according to

$$c_1 = (0.5 - 2.5) \times \frac{i}{I_{\max}} + 2.5,$$
$$c_2 = (2.5 - 0.5) \times \frac{i}{I_{\max}} + 0.5. \tag{30}$$

Based on v_{dq}^i, each particle updates its position according to

$$x_{dq}^i = x_{dq}^{i-1} + v_{dq}^i. \tag{31}$$

Step 4 (fitness update). If $F(\mathbf{x}_d^i) < F(pbest_d^{i-1})$, then set $pbest_d^i = \mathbf{x}_d^i$. Else, if $F(\mathbf{x}_d^i) \geq F(pbest_d^{i-1})$, then set $pbest_d^i = pbest_d^{i-1}$. Set $gbest^i = pbest_{\min}^i$ if $F(pbest_{\min}^i) < F(gbest^{i-1})$. Else, if $F(pbest_{\min}^i) \geq F(gbest^{i-1})$, then set $gbest^i = gbest^{i-1}$. Notice that the numerical objective of PSO, that is, P_e, can be evaluated based on the appointed sequences, such as the preamble (e.g., synchronization pilots) of each frame. Assuming that UWB multipath channels are quasistatic, which means the channel response usually keeps unchanged between several successive frames, and hence, the pilots among the adjacent frames can be also employed to enhance the numerical accuracy.

Step 5 (termination condition check). If the maximum number of iteration, $I_{\max}$, is reached, terminate the search algorithm with the $gbest^{(I_{\max})}$; otherwise, set $i = i + 1$ and go to Step (3).

As is indicated by the PSO algorithm elaborations above, the optimal decision bound $f(F_x, F_y)$ as well as the coefficients η_i is basically independent of any channel parameters. Meanwhile, the derivation process suggests that our characteristic space is not immediately related to specific quantifiable information. Hence, essentially the practical information imperfection or uncertainty has no effect on our final demodulation performance.

4. Numerical Simulations and Evaluation

In this part, we evaluate our PSO-based UWB detection method in a realistic UWB channel through numerical simulations. In our experimental platform, a Gaussian monocycle with duration of $T_p = 0.5$ ns is used as the pulse shaper. The UWB multipath channels are generated by using the channel model in [37] with the real channel tapers and parameters $(1/\Lambda, 1/\lambda, \Gamma, \gamma) = (43, 0.4, 7.1, 4.3)$ ns. Without loss of generality, we also let the number of pulses per symbol $N_s = 1$, that is no repeating coding is used. The timing synchronization has been accurately acquired by the pilot PN sequences with the length of 64. The interested window is determined according to the 95% energy captured criterion, so we focus on the front 150 multipath for example, $N = 150$.

4.1. Features Combinations. As is discussed, the combination coefficients η_i could significantly affect the signal recognition performance, so we firstly investigate the influence of η_i on the PSO-based UWB receiver. In this numerical simulation, the PSO parameters are set as follows: (1) the particle population N_p is set to 40, (2) the inertia weight $w = 0.8$, (3) the acceleration coefficients are constant, $c_1 = c_2 = 2$, (4) the maximum velocity is $v_{\max} = 30$, (5) the maximum iterations $I_{\max}$ is 160, (6) the decision bound function is the quadratic function as given by (24).

Figure 3 plots the representative signals/patterns distributions in the 2-D feature plane under the two different features combination strategies. From the illustrations, we firstly observe that our PSO-based noncoherent algorithm is much superior to ED whose performance can be conveniently evaluated with the decision bound keeping *orthogonal* to F_x axis. Notice that F_x exactly denotes the received power. It is calculated that there are about 300 errors out of the total 6×10^4 transmitted bits in ED. In comparison, the total error of the suggested PSO algorithm is only about 45 when the *ERFC* method is adopted. Additionally, this error number for the *OFC* scheme can be further decreased by 50% basically. Without the features combination coefficients optimization, we note that F_x and F_y are highly correlated under the channel state H_0 from the pattern points in Figure 3(a). As is implied by Figure 3(b) (see the pattern distribution under H_0); however, this correlation can be greatly reduced by optimizing the combination coefficients, which in turn considerably reinforces the final recognition performance. Furthermore, Figure 4 compares the PSO fitness (e.g., bit error rate) under the different feature combination schemes. Based on averaging over 60 independent algorithm realizations, we find that although *ERFC* scheme has the advantage of the smaller particle dimension (e.g., the parameters number) in which the combination coefficients η_i have been predetermined, its convergence is still approximately equivalent to *OFC* method. Moreover, the converged BER in *ERFC* is about 7.5×10^{-4}, while *OFC* is about 3.5×10^{-4}. As a consequence, the *OFC* scheme obviously outperforms *ERFC* in practice. Besides, both our PSO methods are far superior to ED whose BER is about 5×10^{-3}, as indicated by Figure 3.

To comprehensively evaluate the noncoherent detection performance, we also show BER curves for different detection techniques in Figure 5, which are numerically derived through the Monte Carlo method. From this illustration, it is evidently observed that our PSO algorithm can surpass ED by 1.5 dB when the *ERFC* scheme is adopted. By resorting to the *OFC* scheme, the achieved gain in SNR can even approach 2.3 dB. As expected, *OFC* may outperform *ERFC* by 0.8 dB. Moreover, it is noteworthy that the BER curve slop of PSO algorithm is much steeper than ED at high SNR, so we may reasonably expect that the advantage of our proposed scheme may become much more noticeable with the increasing of SNR. Furthermore, if the noise uncertainty

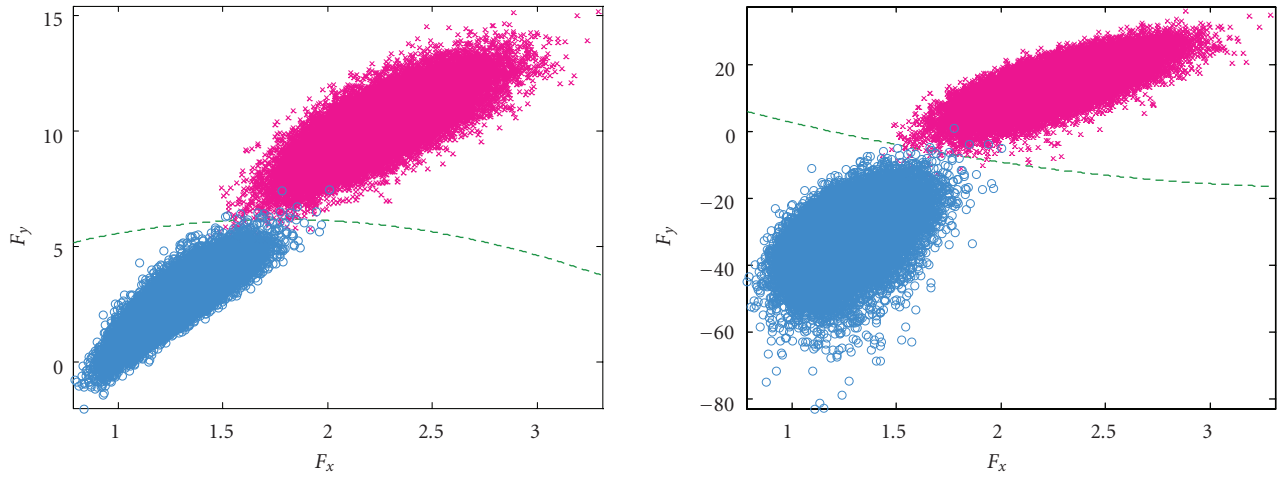

FIGURE 3: Representative signal distribution in 2-D features plane for (a) ERFC scheme, and (b) OFC scheme. The channel E_b/N_o is 12.5 dB. Notice that the data points labeled by "×" denote the channel state H_1, while the *cycles* represent H_0.

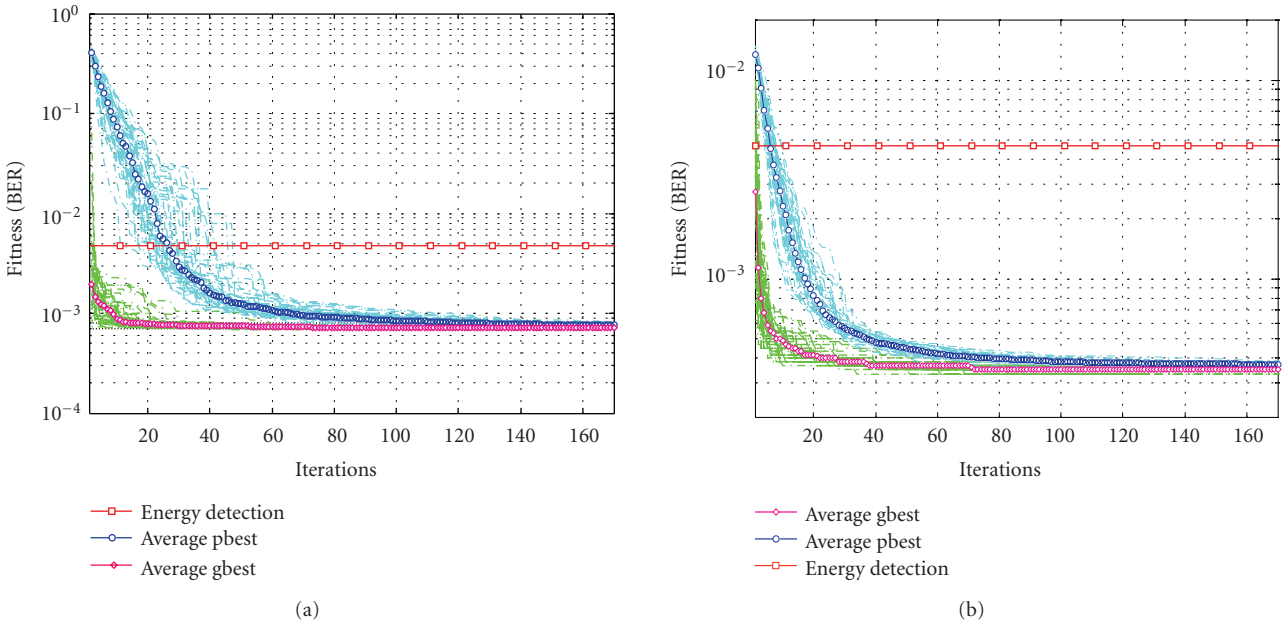

FIGURE 4: The PSO Fitness versus iterations. (a) ERFC scheme; (b) OFC scheme. Notice the E_b/N_o is 12.5 dB.

is taken into consideration, the performance of ED will be declined remarkably, owing to the nonoptimal decision threshold caused by the practical information imperfection [23]. Given that no explicit parametric information is assumed, however, our proposed UWB receiver can operate robustly without any performance degradation. In such a case, the PSO-based UWB demodulator may surpass ED by 5 dB or even better.

The performance of APDP method is also presented in Figure 5 for profound discussions. It is apparent that our presented OFC scheme may surpass APDP by 1dB in high SNR. Observations on BER curve slopes also suggest that this achieved gain may be further improved with the increasing of SNR. Meanwhile, it should be noted that APDP is intrinsic a *centralized* and *semicoherent* algorithm, which needs a prior partial CSI, and requires the network CH continually updating the local channel parameters and further reporting it to each mobile node [41]. Considering the accurate estimation of PDP always consumes considerable network resources, therefore, from the practical aspect, it is in no condition to be applied to the distributed UWB transmissions. Hence, our presented biological algorithm is much superior to the APDP scheme either in transmission performance or in application potential.

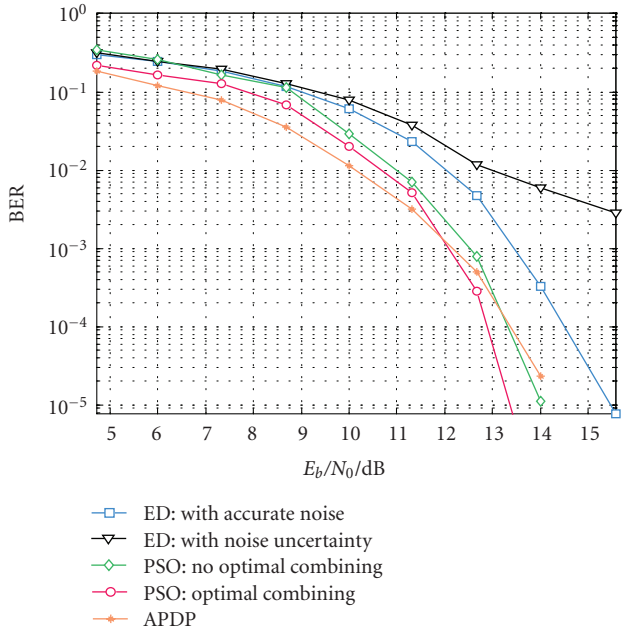

Figure 5: BER curves for different noncoherent methods.

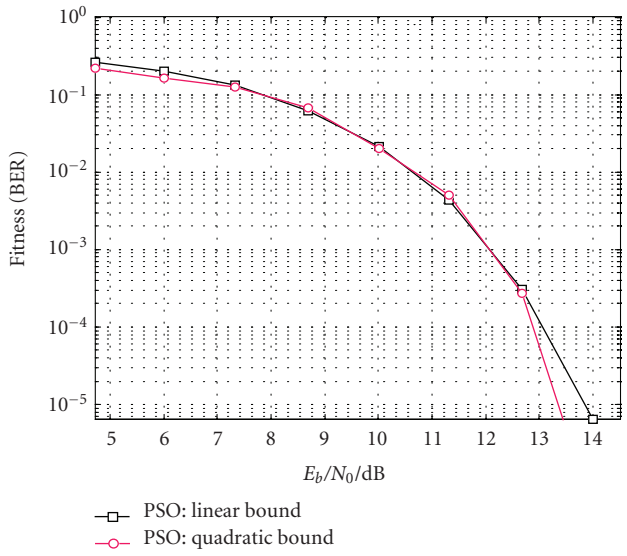

Figure 6: BER performance for different division bound functions 1–4 m.

4.2. Decision Bound. In (23) and (24), we assumed two types decision bounds for PSO-based detection algorithm. This numerical evaluation gives the demodulation performances under the two different bound assumptions. The *OFC* scheme is adopted in this simulation, and other parameters are set the same as in Section 4.1. BER curves corresponding to these two different schemes have been shown in Figure 6, respectively based on the linear function and the quadratic function. We may note that the choice of the decision bounds in PSO-based noncoherent receiver slightly affects the final demodulation performance. In low SNR, this optimization effort is basically rewarded with no SNR gain. Nevertheless, the quadratic function may achieve about 0.4 dB gain compared to the linear function at a high channel SNR.

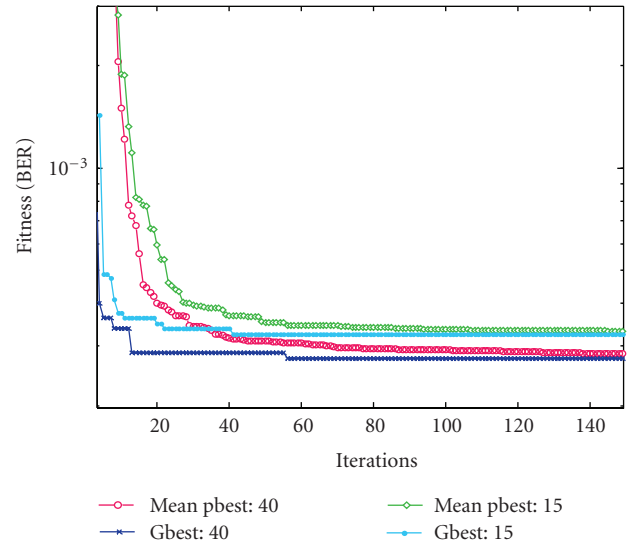

Figure 7: PSO fitness for different number of particle population. The channel SNR is 12.5 dB.

4.3. Particles Population. In this simulation, we investigate the effect of particles population on the final receiving performance. We plot the derived PSO fitness in Figure 7 for the particle size of 15 and 40, respectively. It can be found that the particle population may have little influence on the final demodulation. Specifically, the fitness under the population of 15 is about 3.26×10^{-4}, while the fitness is 2.59×10^{-4} with the population of 40. Hence, in the context of UWB signal detection, the achieved gain seems to be rather limited through the increase of particles population. Considering a large particle population also results in an extraordinary algorithm complexity, therefore, a small particle size can be recommended for the practical UWB detectors.

4.4. Time-Varying Acceleration Coefficients. We compare two different strategies employed for the acceleration coefficients c_1 and c_2 in this experiment. In the first scheme, the acceleration coefficients are set to a constant 2. While in the second TVAC scheme, c_1 and c_2 are both linearly changed according to (30). As is suggested, TVAC comprehensively embodies the PSO philosophy that the particles rely heavily on the private thinking at the beginning and slowly shift to the social cooperation with the increasing of iterations. From the simulation results shown in Figure 8, it is observed that both these two acceleration coefficients schemes can discover the optimal solutions eventually. Nevertheless, the convergence of the mean *pbest* in TVAC is only 12 iterations, while the convergence of the constant method is about 70. So, TVAC is somewhat more computationally efficient from the mean value of *pbest*, and hence is much suitable for some real-time UWB transmissions.

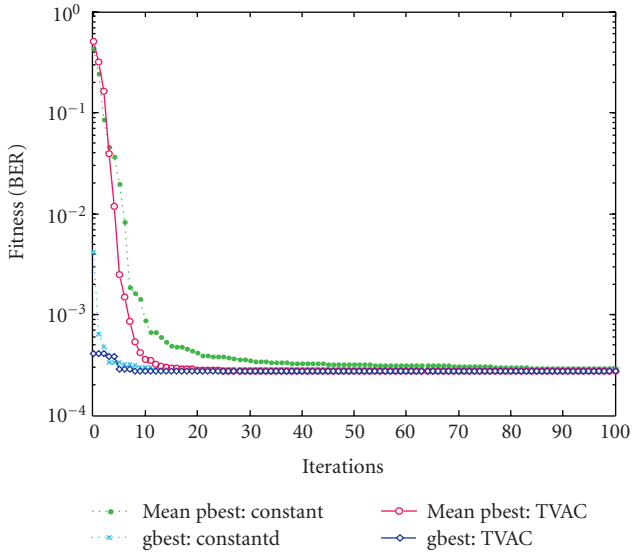

Figure 8: Different strategies of the acceleration coefficients.

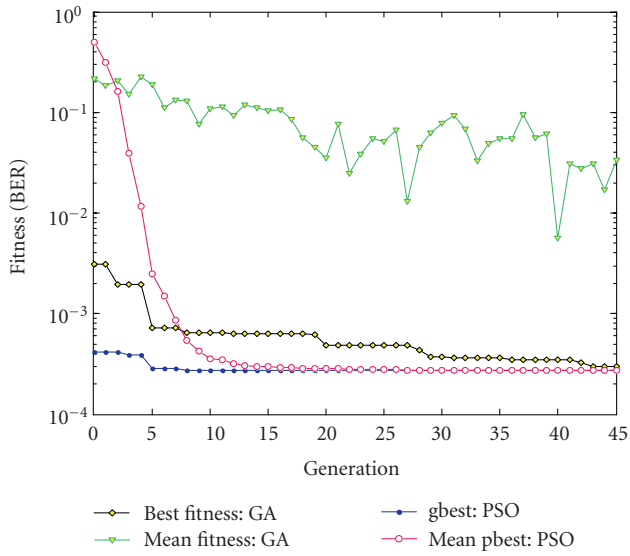

Figure 9: Performance of PSO versus GA.

4.5. Genetic Algorithm. As anther evolutionary algorithm, GA may also find vital applications in various numerical optimizations. In the last numerical experiment, we evaluate these two popular nature inspired optimization techniques in our suggested noncoherent UWB receiver. From Figure 9, we firstly noted that the PSO-based algorithm is much more competitive in convergence. Specifically, the optimal solution can be found by PSO after only 15 iterations. By contrast, the desired generations in GA may even approach 50. This slow convergence characteristic of GA may prevent it from most applications that puts great emphasis on real-time processing, especially for the high-speed online video stream services. Meanwhile, we observed that the optimal fitness of PSO is basically equivalent to GA after algorithm convergence. Therefore, as is reported in most literatures [29], PSO is much superior to GA in our noncoherent UWB detector.

5. Conclusions and Discussions

UWB has intensive military and commercial applications; however, the practical receiver designing still remains a challenging task due to the intensive multipath propagation of UWB channels, which greatly hindered its large-scale application progress. The existing noncoherent UWB receivers can alleviate the impractical requirements on algorithms and hardware structures to some extent, but there is a need to reinforce the detection performance and also overcome the destructive effects from information uncertainty. In this paper, we suggest a noncoherent UWB demodulator inspired by the nature intelligence. Firstly, a characteristic spectrum is developed and certain quantifiable distinguished features are extracted from it. Then, UWB signal detection is transformed to a pattern recognition problem. PSO is adopted to optimize the features combination coefficients and the division bound function. Our biological and nonparametric algorithm is independent of any explicit channel parameters, and hence is much superior to the other noncoherent techniques especially when there is channel noise uncertainty. Based on the characteristic construction, features extraction, and evolutional computation, our proposed PSO-based UWB detector presents a new infrastructure for the nature inspired signal processing, which also benefits the more profound biological applications in engineering problems. In fact, the established characteristic spectrum is somewhat elementary as an early work, and the collected feature is also simple and even intuitive. If the more elegant characteristic spectrum is developed, accompanying the well-established features selection procedure, the achieved gain of this biological technique can be further enhanced, which also remains as an attractive area in future researches.

Acknowledgment

This research was partly supported by the Ministry of Knowledge Economy, Korea, under the ITRC support program supervised by the Institute for Information Technology Advancement (IITA-2009-C1090-0902-0019) This work was supported by NSFC (60772021, 60972079, 60902046), the Research Fund for the Doctoral Program of Higher Education (20070013029), the National High-tech Research and Development Program (863 Program) (2009AA01Z262), the important National Science & Technology Specific Projects (2009ZX03006-006/-009) and the BUPT Excellent Ph.D. Students Foundation (CX201013).

References

[1] M. Z. Win and R. A. Scholtz, "Impulse radio: how it works," *IEEE Communications Letters*, vol. 2, no. 2, pp. 36–38, 1998.

[2] L. Yang and G. B. Giannakis, "Ultra-wideband communications: an idea whose time has come," *IEEE Signal Processing Magazine*, vol. 21, no. 6, pp. 26–54, 2004.

[3] P. Cheolhee and T. S. Rappaport, "Short-range wireless communications for next-generation networks: UWB 60 GHz millimeter-wave wpan, and ZigBee," *IEEE Wireless Communications*, vol. 14, no. 4, pp. 70–78, 2007.

[4] "Multi-band OFDM physical layer proposal for IEEE 802.15 task group 3a," http://www.ieee802.org/15/pub/2003/Jul03/03268r2P802-15_TG3a-Multi-band-CFP-Document.pdf.

[5] P. Withington, H. Fluhler, and S. Nag, "Enhancing homeland security with advanced UWB sensors," *IEEE Microwave Magazine*, vol. 4, no. 3, pp. 51–58, 2003.

[6] S. Nag, M. A. Barnes, T. Payment, and G. W. Holladay, "An ultra-wideband through-wall radar for detecting the motion of people in real time," in *Radar Sensor Technology and data Visualisation*, Proceedings of SPIE, pp. 48–57, Orlando, Fla, USA, April 2002.

[7] T. Zasowski and A. Wittneben, "Performance of UWB receivers with partial CSI using a simple body area network channel model," *IEEE Journal on Selected Areas in Communications*, vol. 27, no. 1, Article ID 4740882, pp. 17–26, 2009.

[8] M. Z. Win and R. A. Scholtz, "Ultra-wide bandwidth time-hopping spread-spectrum impulse radio for wireless multiple-access communications," *IEEE Transactions on Communications*, vol. 48, no. 4, pp. 679–691, 2000.

[9] M. Z. Win and R. A. Scholtz, "Characterization of ultra-wide bandwidth wireless indoor channels: a communication-theoretic view," *IEEE Journal on Selected Areas in Communications*, vol. 20, no. 9, pp. 1613–1627, 2002.

[10] A. F. Molisch, "Ultrawideband propagation channels-theory, measurement, and modeling," *IEEE Transactions on Vehicular Technology*, vol. 54, no. 5, pp. 1528–1545, 2005.

[11] J. Foerster, "Channel modeling sub-committee report final," Tech. Rep. 802.15-02/490, IEEE, 2002.

[12] K. Witrisal, G. Leus, G. J. M. Janssen et al., "Noncoherent ultra-wideband systems: an overview of recent research activities," *IEEE Signal Processing Magazine*, vol. 26, no. 4, pp. 48–66, 2009.

[13] G. Durisi and S. Benedetto, "Comparison between coherent and noncoherent receivers for UWB communications," *EURASIP Journal on Applied Signal Processing*, vol. 2005, no. 3, pp. 1–9, 2005.

[14] V. Lottici, A. D'Andrea, and U. Mengali, "Channel estimation for ultra-wideband communications," *IEEE Journal on Selected Areas in Communications*, vol. 20, no. 9, pp. 1638–1645, 2002.

[15] A. Rajeswaran, V. Srinivasa Somayazulu, and J. R. Foerster, "Rake performance for a pulse based UWB system in a realistic UWB indoor channel," in *Proceedings of the International Conference on Communications (ICC '03)*, vol. 4, pp. 2879–2883, May 2003.

[16] D. Cassioli, M. Z. Win, F. Vatalaro, and A. F. Molisch, "Low complexity Rake receivers in ultra-wideband channels," *IEEE Transactions on Wireless Communications*, vol. 6, no. 4, pp. 1265–1274, 2007.

[17] R. Hoctor and H. Tomlinson, "Delay-hopped transmitted-reference RF communications," in *Proceedings of the IEEE Conference Ultra Wideband Systems and Technologies (UWBST '02)*, pp. 265–270, Baltimore, Md, USA, May 2002.

[18] S. Franz and U. Mitra, "Generalized UWB transmitted reference systems," *IEEE Journal on Selected Areas in Communications*, vol. 24, no. 4 I, pp. 780–786, 2006.

[19] L. Yang and G. B. Giannakis, "Optimal pilot waveform assisted modulation for ultrawideband communications," *IEEE Transactions on Wireless Communications*, vol. 3, no. 4, pp. 1236–1249, 2004.

[20] A. A. D'Amico, U. Mengali, and E. Arias-de-Reyna, "Energy-detection UWB receivers with multiple energy measurements," *IEEE Transactions on Wireless Communications*, vol. 6, no. 7, pp. 2652–2659, 2007.

[21] S. Dubouloz, B. Denis, S. De Rivaz, and L. Ouvry, "Performance analysis of LDR UWB non-coherent receivers in multipath environments," in *Proceedings of the IEEE International Conference on Ultra-Wideband (ICU '05)*, pp. 491–496, September 2005.

[22] W. M. Lovelace and J. K. Townsend, "The effects of timing jitter and tracking on the performance of impulse radio," *IEEE Journal on Selected Areas in Communications*, vol. 20, no. 9, pp. 1646–1651, 2002.

[23] R. Tandra and A. Sahai, "Fundamental limits on detection in low SNR under noise uncertainty," in *Proceedings of the International Conference on Wireless Networks, Communications and Mobile Computing (WirelessCom '05)*, pp. 464–469, Maui, Hawaii, USA, June 2005.

[24] E. Yu and K. S. Sung, "A genetic algorithm for a university weekly courses timetabling problem," *International Transactions in Operational Research*, vol. 9, no. 6, pp. 703–717, 2002.

[25] M. Dorigo, V. Maniezzo, and A. Colorni, "Ant system: optimization by a colony of cooperating agents," *IEEE Transactions on Systems, Man, and Cybernetics, Part B*, vol. 26, no. 1, pp. 29–41, 1996.

[26] D. Dasgupta, Z. Ji, and F. Gonzlez, "Artificial immune system (ais) research in the last five years," in *Proceedings of the International Conference on Evolutionary Computation Conference (CEC '03)*, Canbara, Australia, December 2003.

[27] R. Eberhart and J. Kennedy, "New optimizer using particle swarm theory," in *Proceedings of the 6th International Symposium on Micro Machine and Human Science*, pp. 39–43, October 1995.

[28] J. Kennedy and R. Eberhart, "Particle swarm optimization," in *Proceedings of the IEEE International Conference on Neural Networks (ICNN '95)*, pp. 1942–1948, December 1995.

[29] P. J. Angeline, "Evolutionary optimization versus particle swarm optimization: philosophy and performance difference," in *Proceedings of the Annual Conference on Evolutionary Programming (ACEP '98)*, pp. 601–610, 1998.

[30] K. K. Soo, Y. M. Siu, W. S. Chan, L. Yang, and R. S. Chen, "Particle-swarm-optimization-based multiuser detector for CDMA communications," *IEEE Transactions on Vehicular Technology*, vol. 56, no. 5, pp. 3006–3013, 2007.

[31] W. Yao, S. Chen, S. Tan, and L. Hanzo, "Minimum bit error rate multiuser transmission designs using particle swarm optimisation," *IEEE Transactions on Wireless Communications*, vol. 8, no. 10, Article ID 5288937, pp. 5012–5017, 2009.

[32] H. Liu and J. I. Li, "A particle swarm optimization-based multiuser detection for receive-diversity-aided STBC systems," *IEEE Signal Processing Letters*, vol. 15, pp. 29–32, 2008.

[33] Z. Zhao, Z. Peng, S. Zheng, and J. Shang, "Cognitive radio spectrum allocation using evolutionary algorithms," *IEEE Transactions on Wireless Communications*, vol. 8, no. 9, Article ID 5285159, pp. 4421–4425, 2009.

[34] "First report and order, revision of part 15 of the commission's rules regarding ultra-wideband transmission systems," Tech. Rep. 98-153, FCC, ET Docket, 2002.

[35] A. Papoulis, *Probability, Random Variables, and Stochastic Process*, McGraw-Hill, New York, NY, USA, 4th edition, 2002.

[36] J. G. Proakis, *Digital Communications*, McGraw-Hill, New York, NY, USA, 4th edition, 2001.

[37] IEEE 802.15.SG3a, "Channel modeling sub-committee report final," Tech. Rep. p802.15-02/490r1-SG3a, IEEE, 2003.

[38] M. Z. Win and R. A. Scholtz, "On the robustness of ultra-wide bandwidth signals in dense multipath environments," *IEEE Communications Letters*, vol. 2, no. 2, pp. 51–53, 1998.

[39] E. G. Strom and F. Malmsten, "A maximum likelihood approach for estimating DS-CDMA multipath fading channels," *IEEE Journal on Selected Areas in Communications*, vol. 18, pp. 132–140, January 2000.

[40] J. D. Choi and W. E. Stark, "Performance of ultra-wideband communications with suboptimal receivers in multipath channels," *IEEE Journal on Selected Areas in Communications*, vol. 20, no. 9, pp. 1754–1766, 2002.

[41] B. Li, Z. Zhou, D. Li, and W. Zou, "A novel Parzen probabilistic neural network based on noncoherent detection algorithm for distributed ultra-wideband sensors," *Journal of Network and Computer Applications*, 2011. In press.

[42] M. Weisenhorn and W. Hirt, "ML receiver for pulsed UWB signals and partial channel state information," in *Proceedings of the IEEE International Conference on Ultra-Wideband (ICU '05)*, pp. 180–185, September 2005.

[43] T. Zasowski, F. Troesch, and A. Wittneben, "Partial channel state information and intersymbol interference in low complexity UWB PPM detection," in *Proceedings of the IEEE International Conference on Ultra-Wideband (ICUWB '06)*, pp. 369–374, September 2006.

[44] G. Strang, *Linear Algebra and its Applications*, Harcourt Brace Jovanovich, Orlando, Fla, USA, 1988.

[45] S. Haykin, *Neural Networks: A Comprehensive Foundation*, Prentice Hall, New York, NY, USA, 2nd edition, 1999.

[46] R. O. Duda, P. E. Hart, and D. G. Stork, *Pattern Classification*, John Wiley & Sons, New York, NY, USA, 2nd edition, 2001.

[47] J. Kennedy, "Particle swarm: social adaptation of knowledge," in *Proceedings of the IEEE International Conference on Evolutionary Computation (ICEC '97)*, pp. 303–308, April 1997.

[48] X. Hu, Y. Shi, and R. Eberhart, "Recent advances in particle swarm," in *Proceedings of the Congress on Evolutionary Computation (CEC '04)*, pp. 90–97, June 2004.

[49] Y. Shi and R. Eberhart, "Parameter selection in particle swarm optimization," in *Proceedings of the Annual Conference on Evolutionary Programming (ACEP '98)*, pp. 591–601, 1998.

[50] A. Ratnaweera, S. K. Halgamuge, and H. C. Watson, "Self-organizing hierarchical particle swarm optimizer with time-varying acceleration coefficients," *IEEE Transactions on Evolutionary Computation*, vol. 8, no. 3, pp. 240–255, 2004.